

Autocyclized and Oxidized Forms of SCR7 Induce Cancer Cell Death by Inhibiting Nonhomologous DNA End joining in a Ligase IV Dependent Manner

Supriya V. Vartak¹, Swarup H. Ashok^{2*}, Vidya Gopalakrishnan^{3,4*}, Vindya K.G.^{1*}, Virginie Ropars⁵, Mridula Nambiar¹, Franklin John⁶, Kothanahally S. Sharath Kumar², Rupa Kumari¹, Nitu Kumari¹, Ujjayinee Ray¹, Gudapureddy Radha¹, Depina Dinesh¹, Monica Pandey¹, Hanumappa Ananda^{1,2}, Subhas S. Karki⁷, Mrinal Srivastava¹, Jean Baptiste Charbonnier⁵, Bibha Choudhary^{3**}, Mantelingu Kempegowda^{2**} and Sathees C. Raghavan^{1**}

¹Department of Biochemistry, Indian Institute of Science, Bangalore 560 012, India;

²Department of Chemistry, University of Mysore, Mysuru, India; ³Institute of Bioinformatics and Applied Biotechnology, Electronics City, Bangalore 560 100, India; ⁴Manipal Academy of Higher Education, Manipal, Karnataka, India; ⁵Institute for Integrative Biology of the Cell (I2BC), CEA, CNRS, Univ Paris-Sud, Univ Paris-Saclay, 91198 Gif-sur-Yvette cedex, France; ⁶Department of Chemistry, Sacred Heart College, Kochi 682 013, India; ⁷Department of Pharmaceutical Chemistry, KLE University's College of Pharmacy, Bangalore 560 010, India.

*Equal second authors

**Corresponding authors

Bibha Choudhary	Ph. +91 80 2852 8900 extn 105; Fax:+91 80 2852 8904 e-mail : vibha@ibab.ac.in
Mantelingu Kempegowda	Ph. +91 82 1241 9497; Fax: +91 82 1250 0846 e-mail : kmlingu@gmail.com
Sathees C. Raghavan	Ph. +91 80 2293 2674; Fax: +91 80 2360 0814 e-mail : sathees@iisc.ac.in

Running title: Cyclized and oxidized forms of SCR7 inhibit NHEJ

Received Date : 15-Jun-2018

Revised Date : 23-Aug-2018

Accepted Date : 17-Sep-2018

Article type : Original Articles

This article has been accepted for publication and undergone full peer review but has not been through the copyediting, typesetting, pagination and proofreading process, which may lead to differences between this version and the Version of Record. Please cite this article as doi: 10.1111/febs.14661

This article is protected by copyright. All rights reserved.

Key words: DNA Ligase, Inhibitor of DNA repair, V(D)J recombination, Double-strand break, NHEJ, End-joining, Homologous recombination, CRISPR, Genome editing

Abbreviations

NHEJ, Nonhomologous End Joining; DSB, Double-strand Break; IR, Ionizing Radiation; MMEJ, Microhomology Mediated End Joining; HR, Homologous Recombination; ITC, Isothermal Titration Calorimetry; NMR, Nuclear Magnetic Resonance; DMF, Dimethylformamide; DMSO, Dimethyl sulfoxide; V(D)J, Variable Diversity Joining; MRN complex, MRE11, RAD50 and NBS1; IC₅₀, Inhibitory Concentration 50; HDR, Homology Directed Repair; CRISPR, Clustered Regularly Interspaced Short Palindromic Repeats; Cas, CRISPR associated; TLC, Thin Layer Chromatography; PAGE, Polyacrylamide Gel Electrophoresis, A, Ampicillin; CA, Chloramphenicol-Ampicillin; PS LU, Photostimulated Luminescence Unit; L4/X4, Ligase IV/XRCC4

ABSTRACT

Nonhomologous DNA end joining (NHEJ) is the major DNA double-strand break (DSB) repair pathway in mammals. Previously, we have described a small molecule inhibitor, SCR7, which can inhibit NHEJ in a Ligase IV-dependent manner. Administration of SCR7 within the cells resulted in the accumulation of DNA breaks, cell death and inhibition of tumor growth in mice. In the present study, we report that parental SCR7, which is unstable can get autocyclized into a stable form. Both parental SCR7 and cyclized SCR7 possess the same molecular weight (334.09) and molecular formula (C₁₈H₁₄N₄OS), whereas its oxidized form, SCR7-pyrazine, possesses a different molecular formula (C₁₈H₁₂N₄OS), molecular weight (332.07) and structure. While cyclized form of SCR7 showed robust inhibition of NHEJ *in vitro*, both forms exhibited efficient cytotoxicity. Cyclized and oxidized forms of SCR7 inhibited DNA end joining catalyzed by Ligase IV, whereas their impact was minimal on Ligase III, Ligase I and T4 DNA Ligase-mediated joining. Importantly, both forms inhibited V(D)J recombination, although the effect was more pronounced for SCR7-cyclized. Both forms blocked NHEJ in a Ligase IV-dependent manner leading to accumulation of DSBs within the cells. Although cytotoxicity due to SCR7-cyclized was Ligase IV-specific, the pyrazine form exhibited non-specific cytotoxicity at higher concentrations in Ligase IV-null cells. Finally, we demonstrate that both forms can potentiate the effect of radiation. Thus, we report that cyclized and oxidized forms of SCR7 can inhibit NHEJ in a Ligase IV-dependent manner, although SCR7-pyrazine is less specific to Ligase IV inside the cell.

INTRODUCTION

Failure to repair DNA double-strand breaks (DSBs) could lead to cell death, while their misrepair may result in chromosomal abnormalities and oncogenesis [1-5]. Homologous recombination (HR) and nonhomologous DNA end joining (NHEJ) are two major DSB repair pathways that efficiently repair DSBs in mammals in a cell cycle phase dependent manner [2, 4, 6-9]. Both pathways are well characterized at the mechanistic level and involve different enzymatic machinery. In addition to the classical NHEJ, an alternate NHEJ pathway has been described, that can operate in a microhomology-dependent manner, called microhomology mediated DNA end joining (MMEJ), which utilizes an entirely different set of proteins during DSB joining [6, 10-13].

Among DSB repair pathways, NHEJ corrects majority of the DSBs generated within a cell, as it operates throughout the cell cycle. During NHEJ, KU70/80 proteins bind to the DNA ends and recruit other DNA modifying enzymes such as DNA-PKcs, Artemis and polymerases to DNA ends. DNA Ligase IV/XRCC4 along with XLF and PAXX help in final ligation of DNA ends [2, 4, 6, 7, 14]. In case of MMEJ, Ligase III and/or Ligase I along with other proteins help in repair of DSBs, whereas during HR, the Ligase involved is Ligase I [6, 8-10, 12, 15, 16].

Previously, we have described a novel approach to induce cytotoxicity in cancer cells by inhibiting NHEJ using a small molecule inhibitor, SCR7 [17]. SCR7 blocked NHEJ in a Ligase IV dependent manner both *in vitro* and *ex vivo* leading to accumulation of DNA double-strand breaks (DSBs) within the cells, activating apoptosis. Among the four mouse tumor models studied, three showed significant tumor regression upon treatment with SCR7 [17]. The use of SCR7 as a biochemical inhibitor was also reported for studying the organization and dynamics of NHEJ proteins during a double-strand break and studies involving chromosomal territory relocation during DNA repair [6, 18-20]. Besides, multiple independent studies demonstrated potential of SCR7 in improving precise genome editing [20-28]. A 2 to 19-fold increase in precise genome editing was reported both *ex vivo* and *in vivo*, when SCR7 was used in tandem with CRISPR-Cas9 constructs. Since SCR7 blocked NHEJ mediated repair of Cas9 cleaved chromosomal DNA, precise DSB repair through HR was facilitated.

In the present study, we report that parental SCR7 can get autocyclized to a stable form of SCR7 (SCR7-cyclized) possessing same molecular weight, molecular formula and melting point. This form, upon oxidation can result in SCR7-pyrazine, with a different molecular weight, molecular formula and structure. SCR7-cyclized and SCR7-pyrazine exhibit inhibition of NHEJ in a Ligase IV dependent manner *in vitro*, and are efficient in inducing cytotoxicity in cancer cell lines.

RESULTS

Characterization of SCR7-cyclized and SCR7-pyrazine

In a previous study, we described a small molecule inhibitor, SCR7, that targets the DNA binding domain of Ligase IV, thereby inhibiting the NHEJ pathway [17]. The described structure of SCR7 ($C_{18}H_{14}N_4OS$) consists of two adjacent imine groups making it less stable (SCR7-parental) leading to spontaneous cyclization to give a more stable form of SCR7 (SCR7-cyclized) (Fig. 1A). Several lines of experimentation suggest that reaction of 5,6-diamino-4-hydroxy-2-mercaptopyrimidine with benzaldehyde gives rise to parental SCR7 [5,6-bis((E)-benzylideneamino)-2-mercaptopyrimidin-4-ol] as an intermediate. Autocyclization of parental SCR7 could result in cyclized form of SCR7 (2-mercapto-6,7-diphenyl-7,8-dihydropteridin-4-ol), which upon oxidation leads to the formation of SCR7-pyrazine (2-mercapto-6,7-diphenylpteridin-4-ol) (Fig. 1A).

Incidentally, parental SCR7 and its stable autocyclized form (referred to as SCR7-cyclized, henceforth) are structural isomers and they possess identical chemical formula ($C_{18}H_{14}N_4OS$), molecular weight, exact mass and same number of protons. We observed that like parental SCR7, cyclized form of SCR7 possessed a melting point of 221-225°C, while it was 194-196°C for SCR7-pyrazine. Pyrazine version of SCR7 was formed upon dehydrogenation of SCR7-cyclized and possessed a distinct structure with an exact mass of 333.0798, molecular weight (332.07) and chemical formula ($C_{18}H_{12}N_4OS$).

We synthesized SCR7-cyclized and SCR7-pyrazine through a two-step facile process (Fig. 1B). SCR7-cyclized was obtained with moderate yield in the presence of acetic acid as an additive and DMF as a solvent. Good yield of the oxidative product SCR7-pyrazine was obtained using nitrobenzene as an oxidizing agent and solvent (Fig. 1B). SCR7-cyclized and SCR7-pyrazine were characterized by physical and spectroscopic techniques. SCR6 (L189) was synthesized as described previously [17] and showed singlet peaks at δ 11.97, 11.74 and 9.63 ppm for OH, S-H, CH=N protons, respectively and NH_2 peak was observed at δ 6.69 ppm in the 1H NMR spectrum.

Structural elucidation of SCR7-cyclized was carried out by 1H NMR and ^{13}C NMR spectroscopy (Fig. S1-3). The disappearance of peak at δ 9.63 and appearance of peak at δ 7.49 (s, 1H, NH) & 6.00-6.01 (d, 1H, $J = 2.4$ Hz, benzylic CH) in 1H NMR and ^{13}C signal at δ 52.6 indicates the 6π electrocyclic ring closure reaction to produce SCR7-cyclized. The structure of SCR7-cyclized was further confirmed by D_2O exchange. We observed the disappearance of peak at δ 7.49 and change in the splitting pattern of peak at δ 6.013-6.007 from doublet to singlet indicating the presence of NH adjacent to benzylic CH proton (data not shown). Structural elucidation of SCR7-pyrazine was carried out by 1H NMR, ^{13}C NMR spectroscopy and HRMS (Fig. S4-6). Both NH and benzylic proton peaks were not observed in the 1H NMR spectra of SCR7-pyrazine, which was obtained under mild oxidation

conditions. Thus, SCR7-pyrazine showed disappearance of peak at 7.49 and 6.01-6.00 indicating the dehydrogenation of SCR7-cyclized.

SCR7-cyclized and SCR7-pyrazine inhibit DNA end joining

Previously, we have shown that testicular extracts from mice and rats are proficient in classical NHEJ, and was dependent on Ligase IV, KU70 and KU80 [15, 29-32]. Hence, cell-free repair assay system derived from rat testicular cells was used for comparing the effect of inhibitors on NHEJ (Fig. 1C-G). Results showed that both SCR7-cyclized and SCR7-pyrazine inhibited DNA end joining of [γ - 32 P] ATP oligomeric labeled DNA irrespective of type of DSB used (5' compatible and two different 5'-5' noncompatible DNA ends) (Fig. 1C-G). While SCR7-cyclized showed significant inhibition from a concentration of 100 μ M onwards, SCR7-pyrazine was effective from 200 μ M (Fig. 1C-G). End-joining inhibition mediated by SCR7-cyclized and SCR7-pyrazine was also compared in a plasmid DNA based assay system (Fig 1H,I). *Eco*RI digested pUC18 plasmid DNA was subjected to end-joining reactions using rat testicular extracts in the presence of increasing concentrations of the respective inhibitors (0.1, 0.5, 1 and 2 mM). Results showed a significant inhibition of end-joining by both, SCR7-cyclized and SCR7-pyrazine at comparable concentrations (Fig. 1H,I). Taken together, different forms of SCR7 inhibited DNA-end joining reactions *in vitro*.

DNA Ligase IV is the preferred target for SCR7-cyclized and SCR7-pyrazine

Ligase IV/XRCC4 is the critical enzyme responsible for recreation of phosphodiester bonds during NHEJ [33, 34]. To evaluate whether SCR7-cyclized and SCR7-pyrazine inhibit Ligase IV mediated joining, purified Ligase IV/XRCC4 was used for joining assay [17]. Results showed that although both inhibitors blocked Ligase IV mediated break joining, the effect was more pronounced when SCR7-cyclized was used as compared to SCR7-pyrazine (Fig. 2A). Importantly, ITC studies using Ligase IV/XRCC4, overexpressed and purified from Baculovirus-infected insect cells, showed K_d values of $2.35 \pm 0.76 \mu$ M and $0.5 \pm 0.17 \mu$ M, when incubated with SCR7-cyclized and SCR7-pyrazine, respectively (Fig. 2B). However, a previously described Ligase inhibitor, L189 [35] did not result in any stable binding (Fig. 2B). The specificity of inhibitors was further tested against purified Ligase I, Ligase III and T4 DNA Ligase (Fig. 2C-E). Results showed that neither SCR7-cyclized nor SCR7-pyrazine showed any remarkable inhibition on joining catalyzed by Ligase I, Ligase III or T4 DNA ligase (Fig. 2C-E).

SCR7-cyclized and SCR7-pyrazine inhibit V(D)J recombination inside cells

NHEJ is responsible for repair of DNA double-strand breaks generated during V(D)J recombination, the process by which antibody diversity is generated [36, 37]. Therefore, we examined the impact of Ligase IV inhibitors on V(D)J recombination using previously described extrachromosomal assay system (Fig. 3A) [38-41]. Since both the chemicals induced cell death upon treatment in Nalm6 cells, comparable number of ampicillin colonies were analysed in both treated and vehicle control samples. While SCR7-cyclized treatment resulted in 2.1-fold reduction in coding joint formation, reduction was only 1.5-fold in the case of SCR7-pyrazine upon transfection with pGG51 in pre-B cells (Nalm6) (Fig. 3B). Significant reduction in signal joint formation was also observed (data not shown). Thus, both SCR7-cyclized and SCR7-pyrazine can block NHEJ during V(D)J recombination within the cells, although SCR7-cyclized was more efficient.

Treatment with SCR7-cyclized and SCR7-pyrazine leads to unrepaired DNA breaks inside the cells

Based on above results, we tested whether treatment with Ligase IV inhibitors could block chromosomal NHEJ resulting in accumulation of unrepaired breaks within the cells. HeLa cells were treated with increasing concentrations (50, 100 μ M for 24 h) of SCR7-cyclized and SCR7-pyrazine, and presence of DSBs was determined using γ -H2AX or 53BP1 foci analysis. Results showed significant increase in γ -H2AX and 53BP1 foci formation upon treatment with SCR7-cyclized and SCR7-pyrazine in a concentration dependent manner (Fig. 4A-D), suggesting inhibition of endogenous NHEJ within the cells. Further, comet assay following treatment with SCR7-cyclized and SCR7-pyrazine in Nalm6 cells (100, 250 μ M for 24 h) showed a concentration dependent increase in the tail moment of comets (Fig. 4 E,F), confirming the accumulation of DNA breaks following treatment with SCR7-cyclized and SCR7-pyrazine.

SCR7-cyclized and SCR7-pyrazine can potentiate the effect of γ -radiation leading to enhanced number of DSBs

Our previous studies indicate that SCR7 can potentiate both chemo and radiotherapy [17]. Based on this, we examined whether SCR7-cyclized and SCR7-pyrazine treatment can cause increased levels of radiation-induced DNA breaks, when coadministered, as they inhibit NHEJ in irradiated cells. To test this, HeLa cells were irradiated with γ -rays (1 Gy), or treated with SCR7-cyclized and SCR7-pyrazine form (100 μ M) or coadministered with both. Cells were harvested after 1 h post treatment and evaluated for γ -H2AX and 53BP1 foci formation. Results showed significantly increased levels of γ -H2AX foci, upon coadministration with SCR7-cyclized or SCR7-pyrazine, compared to IR treatment alone

(Fig. 5A,B). Similarly, we also observed significantly high levels of 53BP1 foci, when IR was coadministered with SCR7-cyclized or SCR7-pyrazine (Fig. 5C,D). These results suggest that both SCR7-cyclized and SCR7-pyrazine can block residual NHEJ in IR treated cells leading to increased levels of unrepaired DSBs. Further, we performed a time-course analysis for investigating the repair kinetics of IR-induced DSBs upon coadministration of radiation and inhibitors. Cells were assessed for 53BP1 foci formation at 1, 2, 6 and 12 h recovery period post IR (Fig. 6A-C). Results showed a time-dependent decrease of 53BP1 foci formation in case of radiation alone (post 2 h), suggesting active DSB repair in these cells post irradiation (Fig. 6A-D). Interestingly, treatment with SCR7-cyclized or SCR7-pyrazine alone showed a steady increase in the number of 53BP1 foci within cells (Fig. 6D) suggesting inhibition of endogenous NHEJ in a time-dependent manner leading to accumulation of DSBs. However, coadministration of IR with SCR7-cyclized or SCR7-pyrazine resulted in significant reduction in repair kinetics over time, as compared to samples treated with IR alone (Fig. 6D). Fold change analysis showed that while there was 3.4-fold decrease in number of 53BP1 foci in samples treated with radiation alone at 12 h when compared to 2 h, coadministration of SCR7-cyclized or SCR7-pyrazine with radiation showed only 1.4- and 1.6-fold decrease, respectively (Fig. 6E). Taken together, our results reveal that coadministration of these inhibitors with radiation leads to abrogation of NHEJ-mediated repair process, thus ultimately leading to accumulation of unrepaired DSBs in treated cells.

Different forms of SCR7 induce cytotoxicity in a Ligase IV dependent manner

Previously, we have observed varying levels of cytotoxicity induced by SCR7 in different cancer cell lines [17]. Therefore, we tested the ability of SCR7-pyrazine (0, 50, 100 and 250 μ M for 48 h) in inducing cell death in three different cell lines, MCF7, HeLa and Nalm6. Results showed that SCR7-cyclized and SCR7-pyrazine induced cytotoxicity in a concentration dependent manner, suggesting elevated DSBs following the compound treatment, ultimately leading to cell death (Fig. 7A-C).

In order to evaluate Ligase IV and hence, NHEJ-dependence during cytotoxicity induced by SCR7-cyclized and SCR7-pyrazine, we evaluated their sensitivity in Ligase IV genetic knockout cells, which are deficient in NHEJ [34]. Knock out cell line, N114 and its wild type, Nalm6 cells were treated with increasing concentrations of SCR7-cyclized and SCR7-pyrazine (0, 50, 100 and 250 μ M for 48 h) and evaluated for cytotoxicity (Fig. 7D,E). Results showed that unlike wild type cells, N114 cells did not exhibit any cytotoxicity at 50 and 100 μ M concentrations of SCR7-cyclized. Even at the highest concentration used (250 μ M), there was no significant cell death (Fig. 7D). However, in the case of SCR7-pyrazine treated samples, we observed significant cell death at 250 μ M treated samples, indicating Ligase IV independent cell death at higher concentrations (Fig. 7E). This indicates that the

observed elevated cytotoxicity in the case of SCR7-pyrazine could be contributed by Ligase IV independent mechanism. Thus, although cytotoxicity induced by SCR7-cyclized was due to the presence of Ligase IV, cell death elicited by SCR7-pyrazine may not be entirely dependent on Ligase IV.

Next, we examined whether the increased levels of DSBs in the IR and NHEJ inhibitor coadministered cells could result in elevated cell death. To evaluate this, Nalm6 and HeLa cells were co-treated with IR (1 Gy) and SCR7-cyclized or SCR7-pyrazine (100 μ M) and cell death was monitored using trypan blue assay (Fig. 8A,B). Results showed that similar to SCR7-cyclized, SCR7-pyrazine potentiated the effect of radiation significantly, in both the cell lines tested (Fig. 8A,B). Therefore, our data suggest that increased DSBs following coadministration of IR and NHEJ inhibitors resulted in elevated cytotoxicity in the tested cancer cell lines.

DISCUSSION

Parental SCR7 and SCR7-cyclized possess same molecular weight and formula, unlike SCR7-pyrazine

In a recent study, we had described a small molecule inhibitor, SCR7 that blocks NHEJ, resulting in accumulation of broken DNA within cells, thereby causing tumor regression in mice [17]. In-depth evaluation suggested that parental SCR7, which is less stable, can get spontaneously cyclized into SCR7-cyclized and subsequently oxidized to SCR7-pyrazine.

Both parental SCR7 and SCR7-cyclized have same molecular mass, molecular weight and melting point. Besides, they also possess the same number of protons. However, unlike parental SCR7 and SCR7-cyclized, SCR7-pyrazine has a distinct mass, melting point, number of protons, molecular formula and chemical structure. It appears that reaction conditions, such as temperature, pH and purification strategies can facilitate generation of different forms. A similar scenario, wherein three different forms of Mirin, an inhibitor of MRN complex, with same mass were reported previously [42, 43].

In a recent report, another cyclized form of SCR7, named as SCR7-R was described [44, 45]. However, this form of SCR7 had a melting point of 273-280°C, and molecular weight of 333.0959, which was different compared to SCR7-parental, SCR7-cyclized and SCR7-pyrazine.

SCR7-cyclized and SCR7-pyrazine inhibit NHEJ in a Ligase IV dependent manner with varying efficiencies

Our studies revealed that similar to SCR7-cyclized, treatment with SCR7-pyrazine also resulted in inhibition of DNA end joining in a concentration dependent manner. Importantly, SCR7-pyrazine also inhibited joining of different 5'-5' noncompatible ends, which requires processing of DNA breaks prior to ligation, and is dependent on classical NHEJ proteins [29, 31]. This was also consistent with the observed inhibition of NHEJ by SCR7 [17, 18, 46-49]. Besides, similar to SCR7-cyclized, SCR7-pyrazine also showed specific inhibition of joining catalyzed by Ligase IV and their effect on Ligase III, Ligase I and T4 DNA ligase mediated joining was minimal *in vitro*.

During V(D)J recombination, DNA breaks generated at recombination signal sequence by RAGs are repaired through NHEJ [36, 37]. Upon evaluation of coding joint formation using episomal DNA substrates, we observed that addition of SCR7-cyclized or SCR7-pyrazine significantly reduced recombination frequency. A comparable effect was also observed during signal joint formation; however, among the inhibitors, SCR7-pyrazine was less effective. Hence, SCR7-cyclized and SCR7-pyrazine are potent and effectively inhibited NHEJ in a Ligase IV dependent manner.

Inhibition of NHEJ within the cells can result in accumulation of DNA double-strand breaks [17]. We observed that treatment with SCR7-pyrazine resulted in elevated levels of γ -H2AX foci, which was comparable to that of SCR7-cyclized suggesting unrepaired DSBs. The increased levels of comets seen following SCR7-cyclized and SCR7-pyrazine treatment confirmed the accumulation of DNA breaks within the cells. Previously, we showed that accumulation of DNA breaks could result in cell death [17]. Consistent to that we observed that treatment with both SCR7-cyclized and SCR7-pyrazine culminated in cell death in all the cell lines tested. Interestingly, the sensitivity of cell lines varied and exhibited different IC50 values. Therefore, it is important to point out that various cell lines may exhibit differential sensitivity towards different forms of SCR7. Varying levels of Ligase IV expression, nature of cell type *etc.* could be the factors responsible for it.

The Ligase IV genetic knockout of Nalm6 cells showed no cell death following SCR7-cyclized treatment, while robust cytotoxicity was seen in wild type cells. In contrast, there was significant cell death at high concentrations upon SCR7-pyrazine treatment even in Ligase IV knockout cells, although it was much less compared to wild type cells. This reveals that although cytotoxicity induced by SCR7-cyclized is Ligase IV-dependent, SCR7-pyrazine induced toxicity could be attributed to other targets as well, particularly at high concentrations.

SCR7-cyclized and SCR7-pyrazine could potentiate radiotherapy

Since NHEJ inhibitors can block residual DSB repair following irradiation, this is considered as an ideal strategy to improve the efficacy of radiotherapy and in some instances, chemotherapy. Previously, we showed that SCR7 could improve radio and chemosensitivity in mice tumor models and cancer cell lines [17, 50, 51]. Interestingly, we noted that treatment with SCR7-cyclized or SCR7-pyrazine along with radiation resulted in elevated levels of DSBs, which was higher than either of the agents alone. Further, administration of both the chemicals in combination with radiation resulted in a synergistic effect leading to enhanced cell death. Thus, it appears that similar to cyclized form of SCR7, even its oxidized form can potentiate radiotherapy. In a quantitative study, we observed that cyclized form of SCR7 can bring down the effective dose of radiation by 50-75% in mice (SV/SCR, unpublished). Recently, it has also been reported that SCR7 could improve the efficacy of melphalan by 4 to 7-fold in myeloma patient primary cells [46]. Our studies reveal that SCR7 improves efficacy of temozolomide treatment in glioma primary patient cells several fold (VK/SCR, unpublished). Impact of SCR7-pyrazine in primary patient cells of various cancer types needs to be investigated further.

SCR7 as a tool to improve precise genome editing

In recent years, CRISPR-Cas has become an effective tool for targeted genome editing [20, 52-54]. The DSBs generated by the endonuclease activity of Cas9 results in activation of DSB repair machinery, that can mend the breaks by either NHEJ or HR. NHEJ being an error-prone process can introduce indels (insertions and deletions) at the joining site, thereby disrupting the target locus. Since homology directed repair (HDR) is efficient in NHEJ-deficient cell lines [55], inhibiting NHEJ can lead to upregulation of HDR, and hence effective precise genome editing.

Recent studies have discovered a novel application of SCR7 in CRISPR-Cas mediated genome editing [20, 21, 23]. SCR7 treatment resulted in inhibition of NHEJ, thereby increasing the efficiency (~2-19 fold) of HR-mediated precise genome editing [21, 23, 26]. Considering that both SCR7-cyclized and SCR7-pyrazine could result in inhibition of NHEJ, although with varying efficiencies, they can be harnessed as excellent tools for CRISPR-Cas mediated genome editing. Recent studies have reported the successful use of SCR7 in CRISPR-Cas mediated gene editing in Zebra fish, wherein an increased HDR rate of ~74% was achieved with the combined use of SCR7 and RS-1, a previously reported RAD51 stimulatory compound [56, 57]. It may be interesting to extend their application to other model organisms such as *Drosophila* and *C. elegans* where CRISPR-Cas has been employed.

In conclusion, parental SCR7 can get autocyclized into a stable form, SCR7-cyclized, having the same molecular weight, molecular mass, melting point and number of protons. SCR7-cyclized upon further oxidization results into SCR7-pyrazine having different molecular weight and melting point. Importantly both the forms can inhibit NHEJ in a Ligase IV-dependent manner. Further, the treatment results in accumulation of DSBs inside cells, finally leading to cell death. However, SCR7-cyclized is more specific in its action inside the cells. Since the molecular weight of SCR7-pyrazine (332.07) is less than that of SCR7-cyclized and SCR7-parental (334.09), and SCR7-cyclized is the stable form compared to SCR7-parental, it is evident that the SCR7 used in previous studies described in the literature by different groups demonstrating its effect in genome editing, cancer therapeutics and as a biochemical inhibitor of DSB repair, is most likely the cyclized version.

Materials and methods

Enzymes, chemicals, and reagents

Chemicals and reagents used in the study were purchased from Sigma Chemical Co. (St. Louis, MO, USA) and Sisco Research Laboratories (Andheri (E), Mumbai, India). Restriction enzymes and other DNA-modifying enzymes were obtained from New England Biolabs (Beverly, MA, USA) and Fermentas (Glen Burnie, MD, USA). Culture media were from Lonza (Walkersville, MD, USA), and Himedia (Bengaluru, Karnataka, India). Foetal bovine serum and PenStrep were from Gibco BRL (Gaithersburg, MD, USA) and MP Biomedicals (Santa Ana, CA, USA). Radioisotope-labelled nucleotides were from BRIT (Navi Mumbai, Maharashtra, India). Antibodies were purchased from Santa Cruz Biotechnology (Dallas, TX, USA), Abcam (Cambridge, UK) and Cell Signaling Technology (Danvers, MA, USA).

Plasmids

Plasmid encoding cDNA of human Ligase IV (NCBI accession number BC037491) was purchased from Open Biosystems (Lafayette, CO, USA). Plasmid coexpressing Ligase IV and XRCC4 was a kind gift from Mauro Modesti (France). pGG49 and pGG51 were from M. Lieber, USA. Ligase I and Ligase III α /XRCC1 plasmids were from A. Tomkinson (USA) and K. W. Caldecott (UK), respectively.

Cell lines and culture

HeLa (human cervical cancer), MCF7 (human breast cancer), Nalm6 (Pre B leukemia) and N114 (Ligase IV knockout of Nalm6), were used for the study. HeLa and MCF7 cells were grown in DMEM high glucose with L-glutamine containing 10% FBS while Nalm6 and N114 cells were grown in RPMI medium containing 15% FBS. The cells growing

in log phase were used for transfection [40, 58]. The media was supplemented with 100 µg/ml Penicillin G and streptomycin and incubated at 37°C in a humidified atmosphere containing 5% CO₂.

Nalm6 and N114 [34] cells were from Dr. M. Lieber, USA. MCF7 was from National Centre for Cell Science, Pune, India, and HeLa was from Dr. A. Karande, India.

Oligomeric DNA

Oligomers used in the study were synthesized from Eurofins Genomics (Bengaluru, Karnataka, India) and IDT (San Jose, CA, USA). The oligomers were purified using 10-15% denaturing PAGE, as described [59] (Table S1).

Preparation of oligonucleotide dsDNA substrates

The oligomeric DNA were 5' labelled with [γ -³²P] ATP using T4 Polynucleotide Kinase (see below). SCR19 was annealed to SCR20 or VK11 to generate 5'-5' compatible or 5'-5' noncompatible substrates, respectively [30, 31]. SB1 was annealed to SB5, MP9 to MP10 to generate noncompatible end substrates. In order to prepare the nicked DNA substrate, radiolabelled MS68 was annealed to cold (5' phosphorylated) MS69 and MS70 and annealing was confirmed on a gel.

Chemistry

General information

All work related to analytical thin layer chromatography were performed with E. Merck silica gel 60 F₂₅₄ aluminium plates and were visualized under UV light. The following mobile phases were employed for TLC: chloroform, methanol and hexane, and ethyl acetate in different ratios. The instrumental techniques employed for the characterization of the newly synthesized compounds include ¹H and ¹³C NMR and mass spectroscopy. ¹H and ¹³C-NMR spectra were recorded on an Agilent WM (400 and 100 MHz) Fourier transforms NMR spectrometer in CDCl₃ or DMSO-d₆ solvent using tetramethylsilane (TMS) as internal standard. Chemical shifts were recorded in ppm relative to TMS. Mass and purity were recorded on a LC-MSD-Trap-XCT (Agilent technologies Inc). All the reagents and chemicals used were from Sigma Chemical Co. (St. Louis, MO, USA).

Synthesis of SCR6

SCR6 was synthesised as described before [17]. Briefly, a suspension of 5,6-diamino-4-hydroxy-2-mercaptopyrimidine and benzaldehyde in dimethyl formamide and acetic acid were stirred at room temperature for 16 h. Once the reaction was completed, the reaction mixture was added slowly to ice cold water, solid was precipitated out and collected

by vacuum filtration, washed with water and compound was recrystallized from dimethyl formamide-ethanol to get pure compound, SCR6. Yield=0.93 g (60%); ^1H NMR (400 MHz, DMSO- d_6): δ 11.97 (s, 1H), 11.74 (s, 1H), 9.63 (s, 1H), 7.86 (d, $J=7.2$ Hz, 2H), 7.40–7.32 (m, 3H), 6.69 (s, 2H, NH_2).

Synthesis of SCR7-cyclized

A suspension of SCR6 (0.93 g, 0.0037 mol) and benzaldehyde (0.4 g, 0.0037 mol) in dimethyl formamide (30 mL) and acetic acid (3 mL) was heated at 200°C for 8-10 h. Once the reaction was completed, the reaction mixture was added slowly to ice cold water and a solid was precipitated out which was collected by vacuum filtration, washed with water and compound was recrystallized from dimethyl formamide-ethanol to get pure compound. Yield=0.44 g (35%); Melting point: 221-225°C; ^1H NMR (400 MHz, DMSO- d_6): δ 12.03 (s, 1H), 11.96 (s, 1H), 7.82–7.80 (m, 2H), 7.49 (s, 1H, NH), 7.38–7.24 (m, 8H), 6.01-6.00 (d, $J=2.4$ Hz, 1H, CH); ^{13}C NMR (100 MHz, DMSO- d_6): 173.4, 157.8, 146.9, 143.4, 140.5, 136.5, 130.0, 129.5, 128.9, 128.8, 127.2, 126.7, 104.6, 52.6. m/z (M+H) $^+$ calcd for $\text{C}_{18}\text{H}_{14}\text{N}_4\text{OS}$ 335.08. found: 335.10.

Synthesis of SCR7-pyrazine

Oxidation of SCR7-cyclized (0.44 g, 0.0013 mol) was carried out in nitrobenzene by refluxing for 24 h. After completion of reaction, solids were separated which was collected by vacuum filtration, washed several times with diethyl ether to get pure SCR7-pyrazine. Yield=0.34 g (80%); Melting point: 194-196°C; ^1H NMR (400 MHz, DMSO- d_6): δ 13.40 (s, 1H), 12.80 (s, 1H), 7.40–7.31 (m, 10H); ^{13}C NMR (100 MHz, DMSO- d_6): δ 176.1, 158.8, 156.2, 149.4, 147.3, 138.0, 137.5, 130.1, 130.11, 129.9, 129.1, 128.6, 128.6, 127.5. m/z (M + H) $^+$ Calcd. for $\text{C}_{18}\text{H}_{12}\text{N}_4\text{OS}$ 333.07. found: 333.09.

5' end-labelling of oligomers

5' end-labelling of oligomeric DNA was performed using T4 polynucleotide kinase and [γ - ^{32}P] ATP at 37°C for 1 h as described [10, 58]. Labelled substrates were purified using Sephadex G-25 column and stored at -20°C till use. Radiolabelled duplex DNA was prepared by annealing labelled strand with 5 fold excess of complementary unlabelled strand in 100 mM NaCl and 1 mM EDTA in a boiling water bath, followed by gradual cooling, as described earlier [10, 58].

Ethics statement

Rats were maintained as per the principles and guidelines of the ethical committee for animal care of Indian Institute of Science in accordance with Indian National Law on animal care and use. The experimental design of the present study was approved by Institutional Animal Ethics Committee (Ref. CAF/Ethics/228/2011), Indian Institute of Science, Bangalore, India.

Preparation of cell-free extracts

Rat testicular extract was prepared as described earlier [31, 32]. In brief, testes were collected from male Wistar rats, *Rattus norvegicus* (4–6 weeks old), minced to prepare single cell suspension, and counted using a haemocytometer. Approximately, 2×10^7 cells/ml were pelleted, resuspended in hypotonic buffer (buffer A: 10 mM Tris-HCl (pH 8.0), 1 mM EDTA, 5 mM DTT and 0.5 mM PMSF), and homogenized with protease inhibitors (1 μ g/ml each of leupeptin, aprotinin, and pepstatin). An equal volume of buffer B (50 mM Tris-HCl (pH 8.0), 10 mM MgCl₂, 2 mM DTT, 0.5 mM PMSF, 25% sucrose and 50% glycerol) was added followed by addition of neutralized, saturated ammonium sulfate solution (11% cut off). Supernatant was then collected after centrifugation (3 h at 32,000 g at 2°C), proteins were precipitated by ammonium sulfate (65%) method and dialyzed (buffer C: 25 mM HEPES-KOH (pH 7.9), 0.1 M KCl, 12 mM MgCl₂, 1 mM EDTA, 2 mM DTT and 17% glycerol) for 16 h. Extracts were aliquoted, snap-frozen in liquid nitrogen and stored at -80°C until use.

Expression and purification of proteins

Ligase IV/XRCC4, Ligase III α /XRCC1 and Ligase I were overexpressed in bacteria and purified as described before [17, 60]. Purity and identity of the proteins were confirmed using SDS-PAGE and western blot analysis.

***In vivo* Recombination assay**

The human lymphoid cell line, Nalm6 was cultured and transfected with episomal constructs pGG51 (coding joint) or pGG49 (signal joint) along with SCR7-cyclized or SCR7-pyrazine (100 μ M) by electroporation (300V, 900 μ F, ∞ Ω , 4 mm cuvette thickness) and incubated for 48 h at 37°C [38-41]. Equivalent amount of DMSO served as vehicle control. The DNA was recovered using Hirt harvest method and the reaction products were transformed in *E. coli* DH10B and selected on ampicillin (A) and chloramphenicol-ampicillin (CA) LB agar plates to estimate recombination frequency, as described previously [38-41].

DNA end-joining reaction

NHEJ assay was performed as described before [30, 31, 61-64]. Briefly, cell-free extracts prepared from rat testes were incubated with or without SCR7-cyclized or SCR7-pyrazine (100, 200, 500 μ M and 1 mM) for 30 min at 25°C in NHEJ buffer (25 mM Tris-HCl, [pH 7.5], 75 mM NaCl, 10 mM MgCl₂, 42.5 mM KCl, 0.025% Triton X-100, 100 μ g/ml BSA, 10% PEG, and 5% glycerol). Similarly, purified Ligases were incubated with or without SCR7-cyclized/ SCR7-pyrazine (50, 100, 200, 500 μ M and 1 mM) for 30 min at 25°C. Further, γ -[³²P] ATP labelled DNA oligomeric substrate (4 nM) was added to the reaction mix and incubated for 1 h at 25°C. Reaction was terminated by adding 10 mM EDTA, followed by extraction of DNA products using phenol-chloroform and precipitation method. Purified products were then resolved on a 8% denaturing PAGE, followed by drying and exposing the gel to a PhosphorImager screen. Signals were detected using PhosphorImager (FLA9000, Fuji, Japan) and the data analyzed on Multigaug software (V3.0). The intensity of joined products was quantified and represented as PSLU (Photo-stimulated luminescence units).

Protein purification of Ligase IV/XRCC4 in insect cells

Full length Ligase IV tagged with ten histidines and full length XRCC4 were co-expressed in Sf21 insect cells [65]. The complex was purified by immobilized Ni²⁺ ion affinity chromatography (GE Healthcare), followed by anion exchange chromatography (Resource Q). Purified proteins were dialyzed in 20 mM Tris-HCl pH 8.0, 150 mM NaCl, 5 mM beta-mercaptoethanol, 5% glycerol and stored at -80°C. Protein concentrations are expressed in molarity of 1:2 complexes for Ligase IV/XRCC4.

Ligase IV/XRCC4 interactions with inhibitors by microcalorimetry

Experiments were performed on a VP-ITC calorimeter (Microcal), as described before [66, 67]. All solutions were degassed under vacuum. The reaction cell (1.8 ml) was loaded with between 6 and 16 μ M Ligase IV/XRCC4 solutions. The syringe (500 μ l) was filled with SCR7-cyclized, SCR7-pyrazine, L189 at concentrations between 60 and 160 μ M. For these experiments, L189 was purchased from Tocris Bioscience (3561). Control experiments were performed with SCR7-cyclized solutions injected into buffer. Thermodynamic parameters ΔH , N, and K_a were obtained by nonlinear least-squares fitting of the experimental data using the single set of independent binding sites model of the Origin software provided with the instrument. The free energy of binding (ΔG) and the entropy (ΔS) were determined using the classical thermodynamic formulas: $\Delta G = -RT \ln(K_a)$ and $\Delta G = \Delta H - T\Delta S$. All binding experiments were performed in duplicate at 25°C.

Immunofluorescence

Cells (25,000/ml) were grown on coverslips for 24 h at 37°C, followed by treatment with either SCR7-cyclized or SCR7-pyrazine (50 and 100 µM), and processing for immunofluorescence as described before [17, 51, 64]. Briefly, after 24 h treatment, cells were harvested, fixed (4% paraformaldehyde for 10 min), permeabilized (PBS containing 0.1% Triton X-100 for 5 min) and blocked (PBST containing 0.1% BSA and 10% foetal bovine serum (FBS) for 1 h). Cells were then incubated with anti-γH2AX antibody (1:500; Millipore) or 53BP1 antibody (1: 200; SantaCruz Biotechnologies, USA) overnight at 4°C, washed with PBST and incubated with corresponding biotinylated secondary antibody (1:200) for 2 h. Cells were then washed, incubated with streptavidin-FITC (1:500) for 20 min. The nucleus was counterstained using DAPI/Propidium Iodide, mounted using Glycerol and antifade DABCO, and images were captured using Zeiss Apotome Fluorescence Microscope (Germany) and Zeiss Laser Confocal microscope (Germany).

Experiments were also performed following cotreatment with IR (1 Gy) and SCR7-cyclized or SCR7-pyrazine (100 µM for 1 h) and evaluated post staining with 53BP1 and γ-H2AX antibodies for foci formation. For time-course studies post irradiation, cells were harvested at 1, 2, 6 and 12 h post IR, SCR7-cyclized, SCR7-pyrazine or combination treatment. Cells were fixed using 2% paraformaldehyde and processed for IF using anti-53BP1, as described above.

Neutral comet assay

Comet assay was performed as described previously [17, 51]. Briefly, Nalm6 cells (25,000/ml) were seeded, treated with SCR7-cyclized or SCR7-pyrazine (100 and 250 µM) for 24 h, harvested post treatment and washed with PBS, followed by addition of low melting agarose. The mixture was then spread onto a glass slide and submerged in neutral lysis buffer overnight at 37°C. Slides were then subjected to electrophoresis at 12 V for 25 min, followed by staining with Propidium Iodide. A minimum of 50 cells were imaged per sample for each experiment, scored for comets using Comet Score software and analyzed for % DNA in tail, tail moment and olive moment. Images were captured using Zeiss Apotome Fluorescence Microscope (Germany).

Cytotoxicity assay

Cytotoxicity was assessed using the Trypan Blue dye exclusion assay as described before [68-72]. Briefly, HeLa, MCF7, Nalm6 and N114 cells (25,000/ml) were seeded and treated with SCR7-cyclized or SCR7-pyrazine (50, 100 and 250 µM for 48 h). Cells were harvested, stained with Trypan blue dye, followed by counting of viable cells. Each experiment was repeated a minimum of three times. Experiments were also performed

following cotreatment with IR (1 Gy) and SCR7-cyclized or SCR7-pyrazine (100 μ M for 48 h) and evaluated for cytotoxicity.

Statistical analysis

The results are expressed with standard error mean. All analyses were done with the GraphPad software using one-way ANOVA or Student's t-test. Statistical significance was considered as ns: not significant, * $p < 0.05$, ** $p < 0.005$, *** $p < 0.0001$.

Acknowledgements

We thank Sheetal Sharma and members of SCR laboratory for discussion and comments on the manuscript. We thank central animal facility and confocal facility, IISc for their help. This work was supported by grants from Centre for the Promotion of Advanced Research [Grant No. IFC/5203-4/2015/131] to SCR and JBC, and financial assistance from IISc-DBT partnership programme [DBT/BF/PR/INS/2011-12/IISc] to SCR. JBC is supported by ARC program (SLS220120605310), by ANR (ANR-12-SVSE8-012) and by INCA DomRep (PLBIO 2012-280). SV is supported by Senior Research fellowship from IISc, India, and VG by Senior Research fellowship from CSIR, India.

Conflict of interest

Authors disclose that there is no conflict of interest.

Author contributions

SCR, MK and BC conceived the project and provided reagents. SCR, MK, JBC, SVV, SW and VKG designed the experiments. SVV, VG, VR, MN, RK, NK, UR, GR, DD, MP, BC, HA and MS conducted the biology experiments. SWA, VKG, FJ, KSR conducted the chemistry experiments. SCR, MK, BC, JBC, SSK, SVV, SWA and VKG interpreted the data. SCR, MK and SVV wrote the manuscript.

References

1. Nambiar, M. & Raghavan, S. C. (2011) How does DNA break during chromosomal translocations?, *Nucleic Acids Res.* **39**, 5813-25.
2. Davis, A. J. & Chen, D. J. (2013) DNA double strand break repair via non-homologous end-joining, *Transl Cancer Res.* **2**, 130-143.
3. Friedberg, E. C., Aguilera, A., Gellert, M., Hanawalt, P. C., Hays, J. B., Lehmann, A. R., Lindahl, T., Lowndes, N., Sarasin, A. & Wood, R. D. (2006) DNA repair: from molecular mechanism to human disease, *DNA Repair.* **5**, 986-96.
4. Iliakis, G., Wang, H., Perrault, A. R., Boecker, W., Rosidi, B., Windhofer, F., Wu, W., Guan, J., Terzoudi, G. & Pantelias, G. (2004) Mechanisms of DNA double strand break repair and chromosome aberration formation, *Cytogenet Genome Res.* **104**, 14-20.
5. Javadekar, S. M. & Raghavan, S. C. (2015) Snaps and mends: DNA breaks and chromosomal translocations, *FEBS J.* **282**, 2627-45.
6. Srivastava, M. & Raghavan, S. C. (2015) DNA double-strand break repair inhibitors as cancer therapeutics, *Chem Biol.* **22**, 17-29.
7. Lieber, M. R. (2010) The mechanism of double-strand DNA break repair by the nonhomologous DNA end-joining pathway, *Annu Rev Biochem.* **79**, 181-211.
8. Jasin, M. & Rothstein, R. (2013) Repair of strand breaks by homologous recombination, *Cold Spring Harb Perspect Biol.* **5**, a012740.
9. Wyman, C. & Kanaar, R. (2006) DNA double-strand break repair: all's well that ends well, *Annu Rev Genet.* **40**, 363-83.
10. Sharma, S., Javadekar, S. M., Pandey, M., Srivastava, M., Kumari, R. & Raghavan, S. C. (2015) Homology and enzymatic requirements of microhomology-dependent alternative end joining, *Cell Death Dis.* **6**, e1697.
11. Deriano, L. & Roth, D. B. (2013) Modernizing the nonhomologous end-joining repertoire: alternative and classical NHEJ share the stage, *Annu Rev Genet.* **47**, 433-55.
12. Iliakis, G. (2009) Backup pathways of NHEJ in cells of higher eukaryotes: cell cycle dependence, *Radiother Oncol.* **92**, 310-5.
13. Sfeir, A. & Symington, L. S. (2015) Microhomology-Mediated End Joining: A Back-up Survival Mechanism or Dedicated Pathway?, *Trends Biochem Sci.* **40**, 701-714.
14. Ochi, T., Blackford, A. N., Coates, J., Jhujh, S., Mehmood, S., Tamura, N., Travers, J., Wu, Q., Draviam, V. M., Robinson, C. V., Blundell, T. L. & Jackson, S. P. (2015) DNA repair. PAXX, a paralog of XRCC4 and XLF, interacts with Ku to promote DNA double-strand break repair, *Science.* **347**, 185-8.
15. Tadi, S. K., Sebastian, R., Dahal, S., Babu, R. K., Choudhary, B. & Raghavan, S. C. (2016) Microhomology-mediated end joining is the principal mediator of double-strand break repair during mitochondrial DNA lesions, *Mol Biol Cell.* **27**, 223-35.
16. Manova, V., Singh, S. K. & Iliakis, G. (2012) Processing of DNA double strand breaks by alternative non-homologous end-joining in hyperacetylated chromatin, *Genome Integr.* **3**, 4.
17. Srivastava, M., Nambiar, M., Sharma, S., Karki, S. S., Goldsmith, G., Hegde, M., Kumar, S., Pandey, M., Singh, R. K., Ray, P., Natarajan, R., Kelkar, M., De, A., Choudhary, B. & Raghavan, S. C. (2012) An inhibitor of nonhomologous end-joining abrogates double-strand break repair and impedes cancer progression, *Cell.* **151**, 1474-87.
18. Reid, D. A., Keegan, S., Leo-Macias, A., Watanabe, G., Strande, N. T., Chang, H. H., Oksuz, B. A., Fenyo, D., Lieber, M. R., Ramsden, D. A. & Rothenberg, E. (2015) Organization and dynamics of the nonhomologous end-joining machinery during DNA double-strand break repair, *Proc Natl Acad Sci USA.* **112**, E2575-84.
19. Kulashreshtha, M., Mehta, I. S., Kumar, P. & Rao, B. J. (2016) Chromosome territory relocation during DNA repair requires nuclear myosin 1 recruitment to chromatin mediated by Upsilon-H2AX signaling, *Nucleic Acids Res.*
20. Vartak, S. V. & Raghavan, S. C. (2015) Inhibition of nonhomologous end joining to increase the specificity of CRISPR/Cas9 genome editing, *FEBS J.* **282**, 4289-94.
21. Chu, V. T., Weber, T., Wefers, B., Wurst, W., Sander, S., Rajewsky, K. & Kuhn, R. (2015) Increasing the efficiency of homology-directed repair for CRISPR-Cas9-induced precise gene editing in mammalian cells, *Nat Biotechnol.* **33**, 543-8.
22. Ma, Y., Chen, W., Zhang, X., Yu, L., Dong, W., Pan, S., Gao, S., Huang, X. & Zhang, L. (2016) Increasing the efficiency of CRISPR/Cas9-mediated precise genome editing in rats by inhibiting NHEJ and using Cas9 protein, *RNA Biol.* 1-8.

23. Maruyama, T., Dougan, S. K., Truttmann, M. C., Bilate, A. M., Ingram, J. R. & Ploegh, H. L. (2015) Increasing the efficiency of precise genome editing with CRISPR-Cas9 by inhibition of nonhomologous end joining, *Nat Biotechnol.* **33**, 538-42.
24. Ott de Bruin, L., Yang, W., Capuder, K., Lee, Y. N., Antolini, M., Meyers, R., Gellert, M., Musunuru, K., Manis, J. & Notarangelo, L. (2016) Rapid generation of novel models of RAG1 deficiency by CRISPR/Cas9-induced mutagenesis in murine zygotes, *Oncotarget.* **7**, 12962-74.
25. Sander, J. D. & Joung, J. K. (2014) CRISPR-Cas systems for editing, regulating and targeting genomes, *Nat Biotechnol.* **32**, 347-55.
26. Singh, P., Schimenti, J. C. & Bolcun-Filas, E. (2015) A mouse geneticist's practical guide to CRISPR applications, *Genetics.* **199**, 1-15.
27. Song, J., Yang, D., Xu, J., Zhu, T., Chen, Y. E. & Zhang, J. (2016) RS-1 enhances CRISPR/Cas9- and TALEN-mediated knock-in efficiency, *Nat Commun.* **7**, 10548.
28. Yu, C., Liu, Y., Ma, T., Liu, K., Xu, S., Zhang, Y., Liu, H., La Russa, M., Xie, M., Ding, S. & Qi, L. S. (2015) Small molecules enhance CRISPR genome editing in pluripotent stem cells, *Cell Stem Cell.* **16**, 142-7.
29. Chiruvella, K. K., Sebastian, R., Sharma, S., Karande, A. A., Choudhary, B. & Raghavan, S. C. (2012) Time-dependent predominance of nonhomologous DNA end-joining pathways during embryonic development in mice, *J Mol Biol.* **417**, 197-211.
30. Kumar, T. S., Kari, V., Choudhary, B., Nambiar, M., Akila, T. S. & Raghavan, S. C. (2010) Anti-apoptotic protein BCL2 down-regulates DNA end joining in cancer cells, *J Biol Chem.* **285**, 32657-70.
31. Sharma, S., Choudhary, B. & Raghavan, S. C. (2011) Efficiency of nonhomologous DNA end joining varies among somatic tissues, despite similarity in mechanism, *Cell Mol Life Sci.* **68**, 661-76.
32. Sathees, C. R. & Raman, M. J. (1999) Mouse testicular extracts process DNA double-strand breaks efficiently by DNA end-to-end joining, *Mutat Res.* **433**, 1-13.
33. Grawunder, U., Wilm, M., Wu, X., Kulesza, P., Wilson, T. E., Mann, M. & Lieber, M. R. (1997) Activity of DNA ligase IV stimulated by complex formation with XRCC4 protein in mammalian cells, *Nature.* **388**, 492-5.
34. Grawunder, U., Zimmer, D., Fugmann, S., Schwarz, K. & Lieber, M. R. (1998) DNA ligase IV is essential for V(D)J recombination and DNA double-strand break repair in human precursor lymphocytes, *Mol Cell.* **2**, 477-84.
35. Chen, X., Zhong, S., Zhu, X., Dziegielewska, B., Ellenberger, T., Wilson, G. M., MacKerell, A. D., Jr. & Tomkinson, A. E. (2008) Rational design of human DNA ligase inhibitors that target cellular DNA replication and repair, *Cancer Res.* **68**, 3169-77.
36. Gellert, M. (2002) V(D)J recombination: RAG proteins, repair factors, and regulation, *Annu Rev Biochem.* **71**, 101-32.
37. Schatz, D. G. & Swanson, P. C. (2011) V(D)J recombination: mechanisms of initiation, *Annu Rev Genet.* **45**, 167-202.
38. Raghavan, S. C., Kirsch, I. R. & Lieber, M. R. (2001) Analysis of the V(D)J recombination efficiency at lymphoid chromosomal translocation breakpoints, *J Biol Chem.* **276**, 29126-33.
39. Raghavan, S. C., Swanson, P. C., Wu, X., Hsieh, C. L. & Lieber, M. R. (2004) A non-B-DNA structure at the Bcl-2 major breakpoint region is cleaved by the RAG complex, *Nature.* **428**, 88-93.
40. Nambiar, M. & Raghavan, S. C. (2012) Mechanism of fragility at BCL2 gene minor breakpoint cluster region during t(14;18) chromosomal translocation, *J Biol Chem.* **287**, 8688-701.
41. Raghavan, S. C., Tong, J. & Lieber, M. R. (2006) Hybrid joint formation in human V(D)J recombination requires nonhomologous DNA end joining, *DNA Repair.* **5**, 278-85.
42. Garner, K. M., Pletnev, A. A. & Eastman, A. (2009) Corrected structure of mirin, a small-molecule inhibitor of the Mre11-Rad50-Nbs1 complex, *Nat Chem Biol.* **5**, 129-30; author reply 130.
43. Dupre, A., Boyer-Chatenet, L., Sattler, R. M., Modi, A. P., Lee, J. H., Nicolette, M. L., Kopelovich, L., Jasin, M., Baer, R., Paull, T. T. & Gautier, J. (2008) A forward chemical genetic screen reveals an inhibitor of the Mre11-Rad50-Nbs1 complex, *Nat Chem Biol.* **4**, 119-25.
44. Greco, G. E., Matsumoto, Y., Brooks, R. C., Lu, Z., Lieber, M. R. & Tomkinson, A. E. (2016) SCR7 is neither a selective nor a potent inhibitor of human DNA ligase IV, *DNA Repair.* **43**, 18-23.
45. Greco, G. E., Conrad, A. Z., Johnston, M. A., Li, Q. & Tomkinson, E. E. (2016) Synthesis and structure determination of SCR7, a DNA ligase inhibitor, *Tetrahedron Let.* **57**, 3204-3207.
46. Gkatzamanidou, M., Terpos, E., Bamia, C., Munshi, N. C., Dimopoulos, M. A. & Souliotis, V. L. (2016) DNA repair of myeloma plasma cells correlates with clinical outcome: the effect of the nonhomologous end-joining inhibitor SCR7, *Blood.* **128**, 1214-25.
47. Tripathi, V., Agarwal, H., Priya, S., Batra, H., Modi, P., Pandey, M., Saha, D., Raghavan, S. C. & Sengupta, S. (2018) MRN complex-dependent recruitment of ubiquitylated BLM helicase to DSBs negatively regulates DNA repair pathways, *Nat Commun.* **9**, 1016.

48. Reid, D. A., Conlin, M. P., Yin, Y., Chang, H. H., Watanabe, G., Lieber, M. R., Ramsden, D. A. & Rothenberg, E. (2017) Bridging of double-stranded breaks by the nonhomologous end-joining ligation complex is modulated by DNA end chemistry, *Nucleic Acids Res.* **45**, 1872-1878.
49. Kulashreshtha, M., Mehta, I. S., Kumar, P. & Rao, B. J. (2016) Chromosome territory relocation during DNA repair requires nuclear myosin 1 recruitment to chromatin mediated by Upsilon-H2AX signaling, *Nucleic Acids Res.* **44**, 8272-91.
50. John, F., George, J., Srivastava, M., Hassan, P. A., Aswal, V. K., Karki, S. S. & Raghavan, S. C. (2015) Pluronic copolymer encapsulated SCR7 as a potential anticancer agent, *Faraday Discussion.* **177**, 155-61.
51. John, F., George, J., Vartak, S. V., Srivastava, M., Hassan, P. A., Aswal, V. K., Karki, S. S. & Raghavan, S. C. (2015) Enhanced efficacy of pluronic copolymer micelle encapsulated SCR7 against cancer cell proliferation, *Macromol Biosci.* **15**, 521-34.
52. Doudna, J. A. & Charpentier, E. (2014) Genome editing. The new frontier of genome engineering with CRISPR-Cas9, *Science.* **346**, 1258096.
53. Wang, H., La Russa, M. & Qi, L. S. (2016) CRISPR/Cas9 in Genome Editing and Beyond, *Ann Rev Biochem.* **85**, 227-64.
54. Barrangou, R., Fremaux, C., Deveau, H., Richards, M., Boyaval, P., Moineau, S., Romero, D. A. & Horvath, P. (2007) CRISPR provides acquired resistance against viruses in prokaryotes, *Science.* **315**, 1709-12.
55. Pierce, A. J., Hu, P., Han, M., Ellis, N. & Jasin, M. (2001) Ku DNA end-binding protein modulates homologous repair of double-strand breaks in mammalian cells, *Genes Dev.* **15**, 3237-42.
56. Zhang, Y., Zhang, Z. & Ge, W. (2018) An efficient platform for generating somatic point mutations with germline transmission in the zebrafish by CRISPR/Cas9-mediated gene editing, *J Biol Chem.* **293**, 6611-6622.
57. Yang, Z., Chen, S., Xue, S., Li, X., Hu, J., Sun, Z. & Cui, H. (2018) Injection of an SV40 transcriptional terminator causes embryonic lethality: a possible zebrafish model for screening nonhomologous end-joining inhibitors, *Onco Targets Therapy.* **11**, 4945-4953
58. Nambiar, M., Srivastava, M., Gopalakrishnan, V., Sankaran, S. K. & Raghavan, S. C. (2013) G-quadruplex structures formed at the HOX11 breakpoint region contribute to its fragility during t(10;14) translocation in T-cell leukemia, *Mol Cell Biol.* **33**, 4266-81.
59. Kumari, R., Nambiar, M., Shanbagh, S. & Raghavan, S. C. (2015) Detection of G-quadruplex DNA using primer extension as a tool, *PLoS One.* **10**, e0119722.
60. Pandey, M., Kumar, S., Goldsmith, G., Srivastava, M., Elango, S., Shameem, M., Bannerjee, D., Choudhary, B., Karki, S. S. & Raghavan, S. C. (2017) Identification and characterization of novel ligase I inhibitors, *Mol Carcinogen.* **56**, 550-566.
61. Kavitha, C. V., Nambiar, M., Narayanaswamy, P. B., Thomas, E., Rathore, U., Ananda Kumar, C. S., Choudhary, B., Rangappa, K. S. & Raghavan, S. C. (2013) Propyl-2-(8-(3,4-difluorobenzyl)-2',5'-dioxo-8-azaspiro[bicyclo[3.2.1] octane-3,4'-imidazolidine]-1'-yl) acetate induces apoptosis in human leukemia cells through mitochondrial pathway following cell cycle arrest, *PLoS One.* **8**, e69103.
62. Chiruvella, K. K., Panjamurthy, K., Choudhary, B., Joy, O. & Raghavan, S. C. (2010) Methyl angolensate from callus of Indian redwood induces cytotoxicity in human breast cancer cells, *Int J Biomed Sci.* **6**, 182-94.
63. Srivastava, S., Dahal, S., Naidu, S. J., Anand, D., Gopalakrishnan, V., Kooloth Valappil, R. & Raghavan, S. C. (2017) DNA double-strand break repair in *Penaeus monodon* is predominantly dependent on homologous recombination, *DNA Res.* **24**, 117-128.
64. Sebastian, R. & Raghavan, S. C. (2016) Induction of DNA damage and erroneous repair can explain genomic instability caused by endosulfan, *Carcinogenesis.* **37**, 929-40.
65. Sari, D., Gupta, K., Thimiri Govinda Raj, D. B., Aubert, A., Drncova, P., Garzoni, F., Fitzgerald, D. & Berger, I. (2016) The MultiBac Baculovirus/Insect Cell Expression Vector System for Producing Complex Protein Biologics, *Adv Exp Med Biol.* **896**, 199-215.
66. Malivert, L., Ropars, V., Nunez, M., Drevet, P., Miron, S., Faure, G., Guerois, R., Moron, J. P., Revy, P., Charbonnier, J. B., Callebaut, I. & de Villartay, J. P. (2010) Delineation of the Xrcc4-interacting region in the globular head domain of cernunnos/XLF, *J Biol Chem.* **285**, 26475-83.
67. Ropars, V., Drevet, P., Legrand, P., Baconnais, S., Amram, J., Faure, G., Marquez, J. A., Pietrement, O., Guerois, R., Callebaut, I., Le Cam, E., Revy, P., de Villartay, J. P. & Charbonnier, J. B. (2011) Structural characterization of filaments formed by human Xrcc4-Cernunnos/XLF complex involved in nonhomologous DNA end-joining, *Proc Natl Acad Sci. USA.* **108**, 12663-8.
68. Moorthy, B. T., Ravi, S., Srivastava, M., Chiruvella, K. K., Hemlal, H., Joy, O. & Raghavan, S. C. (2010) Novel rhodanine derivatives induce growth inhibition followed by apoptosis, *Bioorg Med Chem Lett.* **20**, 6297-301.

69. Srivastava, M., Hegde, M., Chiruvella, K. K., Koroth, J., Bhattacharya, S., Choudhary, B. & Raghavan, S. C. (2014) Sapodilla plum (*Achras sapota*) induces apoptosis in cancer cell lines and inhibits tumor progression in mice, *Scientific Rep.* **4**, 6147.
70. Srivastava, S., Somasagara, R. R., Hegde, M., Nishana, M., Tadi, S. K., Srivastava, M., Choudhary, B. & Raghavan, S. C. (2016) Quercetin, a Natural Flavonoid Interacts with DNA, Arrests Cell Cycle and Causes Tumor Regression by Activating Mitochondrial Pathway of Apoptosis, *Scientific Rep.* **6**, 24049.
71. Iyer, D., Vartak, S. V., Mishra, A., Goldsmith, G., Kumar, S., Srivastava, M., Hegde, M., Gopalakrishnan, V., Glenn, M., Velusamy, M., Choudhary, B., Kalakonda, N., Karki, S. S., Surolia, A. & Raghavan, S. C. (2016) Identification of a novel BCL2-specific inhibitor that binds predominantly to the BH1 domain, *FEBS J.* **283**, 3408-37.
72. Vartak, S. V., Iyer, D., Santhoshkumar, T. R., Sharma, S., Mishra, A., Goldsmith, G., Srivastava, M., Srivastava, S., Karki, S. S., Surolia, A., Choudhary, B. & Raghavan, S. C. (2017) Novel BCL2 inhibitor, Disarib induces apoptosis by disruption of BCL2-BAK interaction, *Biochem Pharmacol.* **131**, 16-28.

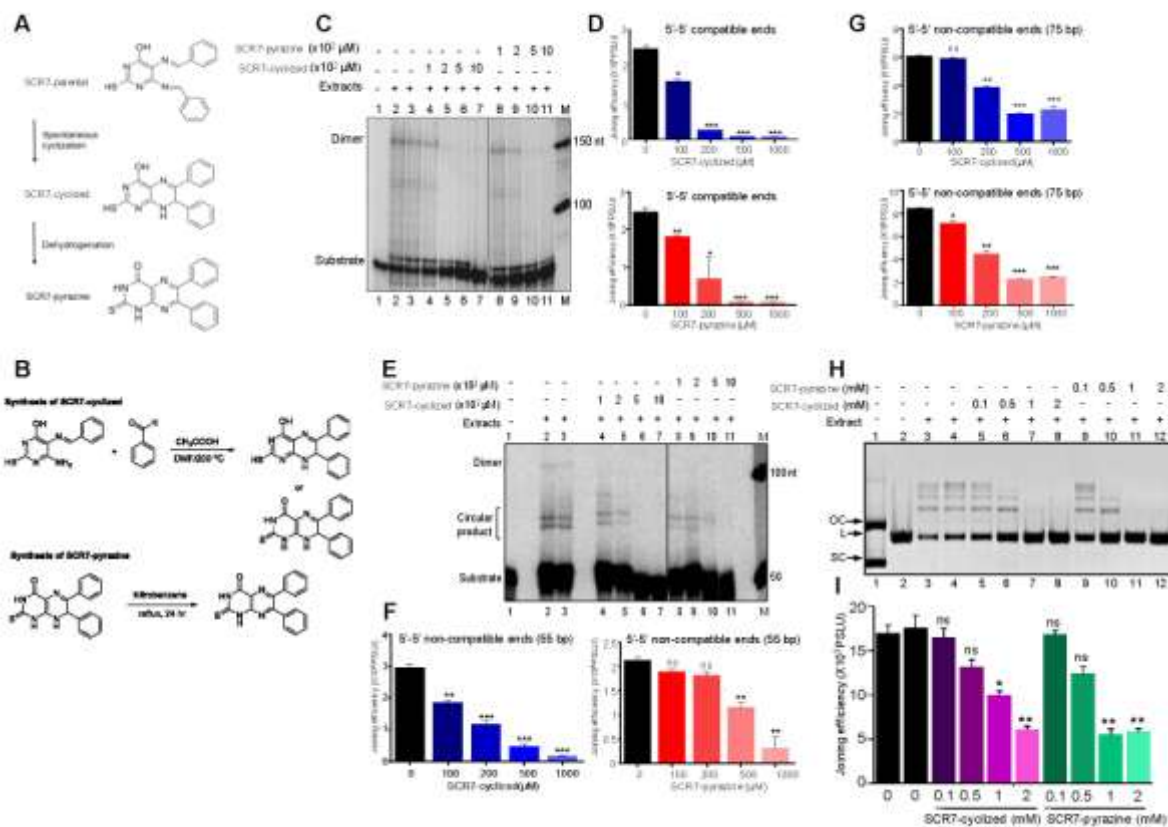


Figure 1

Figure 1. Chemical structures of different forms of SCR7 and their effect on end joining of DNA double-strand breaks. **A.** Parental SCR7 upon autocyclization can get converted into a stable form of SCR7 (SCR7-cyclized), which following dehydrogenation is converted into SCR7-pyrazine. **B.** Synthesis of SCR7-cyclized and SCR7-pyrazine. **C.** Representative PAGE profile showing effect of SCR7-cyclized and SCR7-pyrazine on joining of DSBs with 5'-5' compatible termini catalyzed by rat testicular extracts (n=4). 'M' represents 50 bp ladder. **D.** Bar graph depicting DNA end-joining efficiency upon treatment with SCR7-cyclized and SCR7-pyrazine for 5'-5' compatible DNA substrate. **E.** PAGE profile showing effect of SCR7-cyclized and SCR7-pyrazine on joining of a 55 bp DNA substrate possessing 5'-5' noncompatible ends catalyzed by rat testicular extracts. **F.** Bar graph showing quantification of joining efficiency for 5'-5' noncompatible end substrates as determined using MultiGauge based on multiple gels (n=3). **G.** Bar graph showing quantification of joining efficiency of a 75 bp DNA substrate possessing 5'-5' noncompatible ends. **H.** Representative gel image showing inhibition of DNA end-joining by SCR7-cyclized and SCR7-pyrazine when a linear (*EcoRI*) plasmid DNA was used as a substrate. pUC18 plasmid DNA was digested using *EcoRI* to generate compatible ends. Rat testicular extract was incubated with increasing concentrations of SCR7-cyclized and SCR7-pyrazine (0.1, 0.5, 1 and 2 mM) for 30 min at 25°C. Linear pUC18 DNA substrate was then added and the

Accepted Article

reaction was allowed to proceed for 1 h at 25°C. Joined products were purified and resolved on a 1% agarose gel. **I.** Bar graph depicting quantification of joined products as quantified using MultiGauge software. Each experiment was repeated (n=3), joined product intensity quantified, and presented as bar graphs. In all panels, bar diagram represents mean \pm SEM (ns: not significant, *p < 0.05, **p < 0.005, ***p < 0.0001). In all cases, significance was calculated using the Student's t-test in GraphPad Prism software.

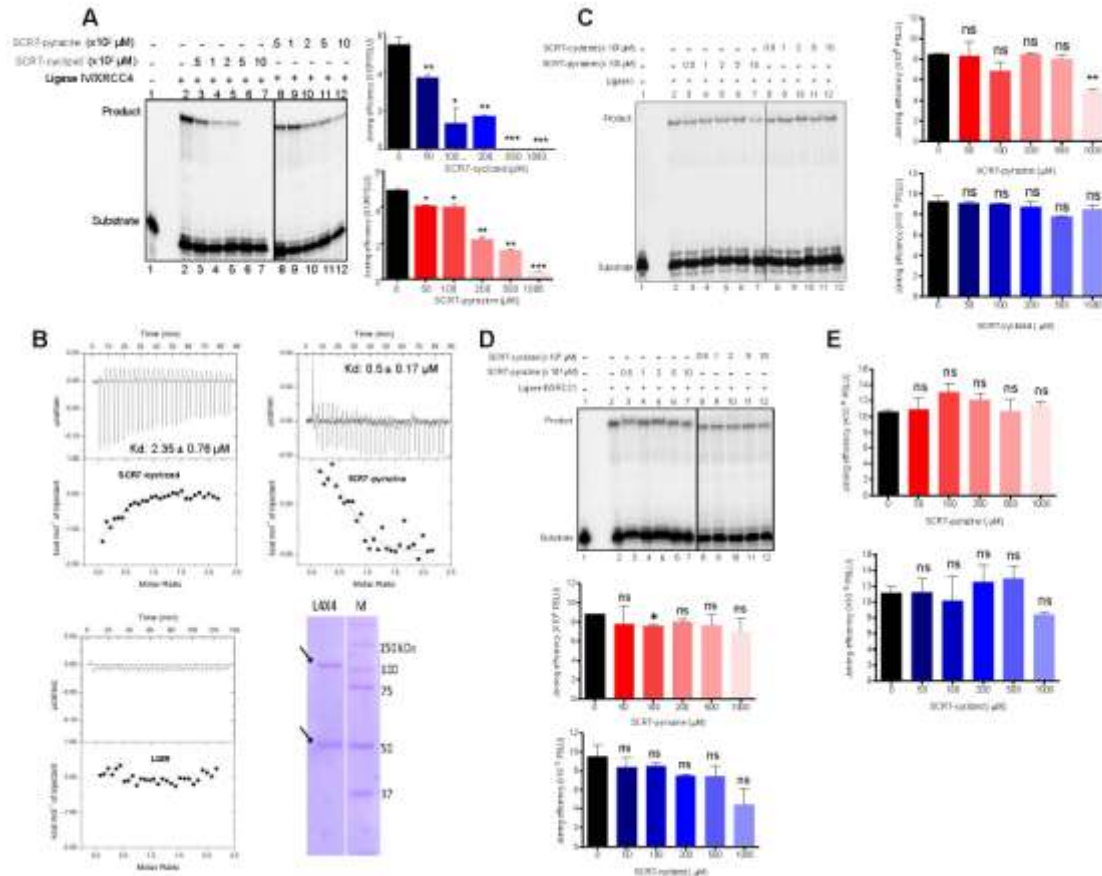


Figure 2

Figure 2. Analysis of specificity of SCR7-cyclized and SCR7-pyrazine against different mammalian DNA Ligases. **A.** Effect of SCR7-cyclized and SCR7-pyrazine on DNA joining catalyzed by purified DNA Ligase IV/XRCC4 on a DNA substrate bearing nick. In each case, 50, 100, 200, 500 and 1000 μM inhibitor concentrations were tested. Each experiment was repeated ($n=3$) and the joining efficiency was quantified and plotted as a bar graph (right panel). **B.** Measurements of interactions by microcalorimetry (ITC). The interactions between Ligase IV/XRCC4 and SCR7-cyclized, SCR7-pyrazine or L189 are shown. Thermograms (top) and isotherm of titrations (below) have been depicted for each titration. PAGE profile of purified Ligase IV/XRCC4 (L4/X4) proteins purified from Baculovirus infected insect cells is also shown. **C.** Denaturing PAGE profile showing effect of SCR7-cyclized and SCR7-pyrazine on joining of nicked DNA catalyzed by Ligase I. Bar graph with error bars is shown on the right. **D.** Effect of SCR7-cyclized and SCR7-pyrazine on DNA joining catalyzed by Ligase III/XRCC1. Bar graph with error bars is also presented. **E.** Bar graph depicting effect of SCR7-cyclized and SCR7-pyrazine on joining of double-stranded DNA catalyzed by T4 DNA Ligase. In each case ($n=3$), the joining efficiency is plotted as a bar graph showing mean \pm SEM (ns: not significant, * $p < 0.05$, ** $p < 0.005$, *** $p < 0.0001$). In all cases, significance was calculated using the Student's t-test in GraphPad Prism software.

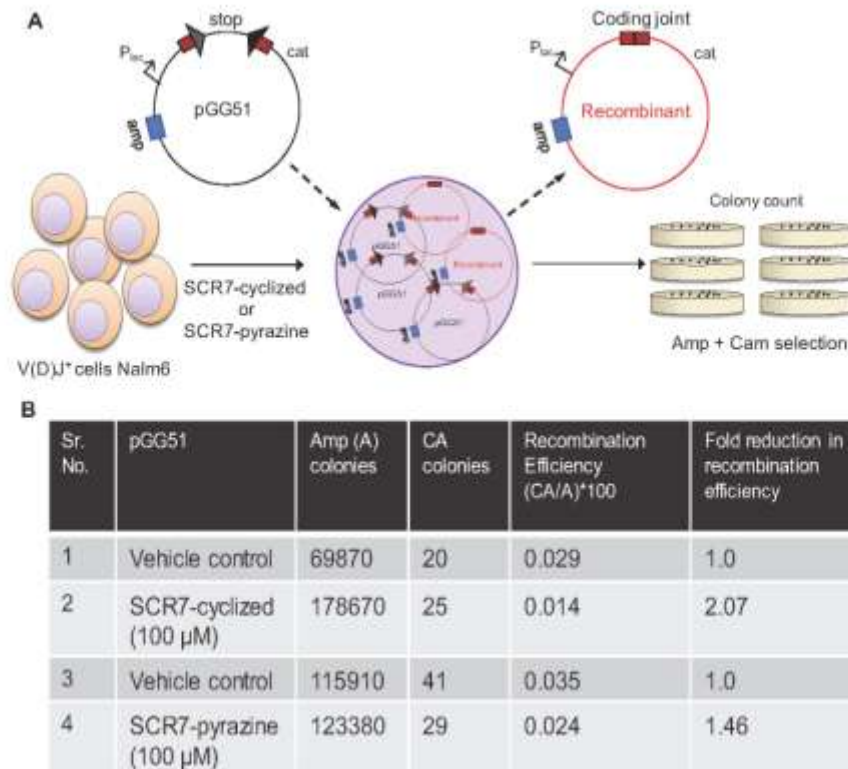


Figure 3

Figure 3. Evaluation of efficiency of V(D)J recombination upon treatment with SCR7-cyclized or SCR7-pyrazine. **A.** Schematic presentation showing human V(D)J recombination assay. The diagram depicts transfection of episome into a human pre-B cell line, Nalm6, active for V(D)J recombination, in presence of SCR7-cyclized or SCR7-pyrazine (100 μ M). DMSO treated cells served as vehicle control. After 48 h inside the cells, the episomes were harvested by Hirt harvest method and transformed into *E. coli DH10B* for detection of recombinants on LB agar plates containing ampicillin and chloramphenicol (Amp + Cam). The recombination is depicted between a consensus 12- (grey triangle) and 23- (black triangle) signal of pGG51, leading to coding joint formation. “cat” denotes the chloramphenicol acetyl transferase gene, and “stop” denotes the prokaryotic transcription terminator. The *E. coli* lac promoter is denoted as “P_{lac}”. **B.** Table summarizing effect of SCR7-cyclized and SCR7-pyrazine on V(D)J recombination in pre-B cells. The episome, pGG51 was transfected into Nalm6 cell line, and the recombination efficiency was tested following transformation into *E. coli*. The recombination frequency is calculated by the formula: (CA/A)x100, where the number of colonies obtained on ampicillin plate (A) and chloramphenicol-ampicillin (CA) selective media for the episomal substrate pGG51. Fold change in recombination following treatment with SCR7-cyclized and SCR7-pyrazine is also shown. Transfections were performed (n=3) followed by multiple transformations using each batch.

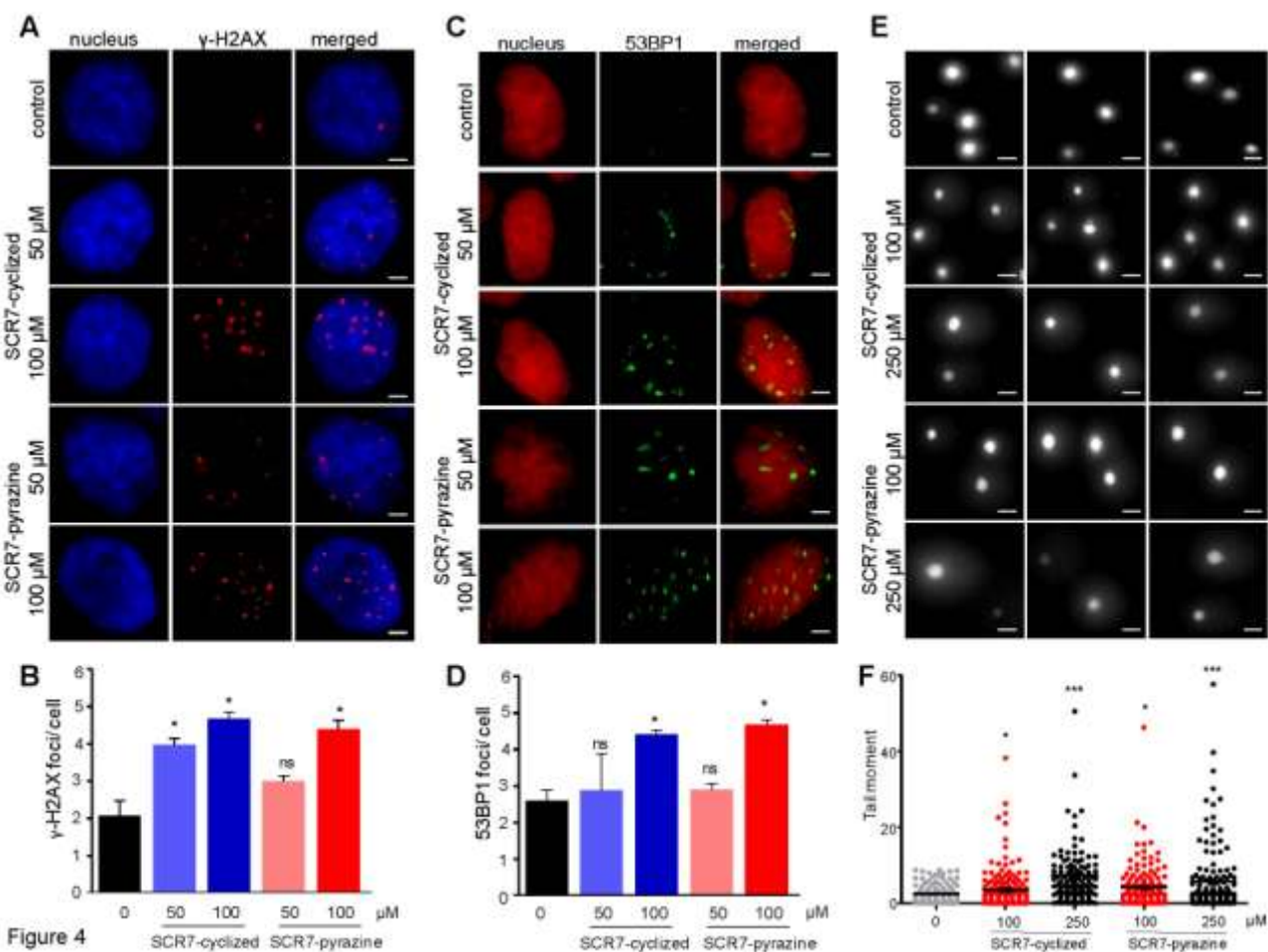


Figure 4. Detection of DNA double-strand breaks within cells upon treatment with SCR7-cyclized and SCR7-pyrazine. **A.** Representative images showing γ -H2AX foci formation in HeLa cells following treatment with SCR7-cyclized and SCR7-pyrazine (50 μ M and 100 μ M) for 24 h. DMSO was used as a vehicle control. γ -H2AX is depicted by Alexa-fluor 568 staining (red), whereas nucleus is counterstained using DAPI (blue). Each experiment was repeated independent times ($n=3$). The scale bar represents 0.2 μ m. **B.** Bar graph depicting γ -H2AX foci per cell representing mean \pm SEM (ns: not significant, * $p < 0.05$, ** $p < 0.005$, *** $p < 0.0001$). In all cases, significance was calculated using the Student's t-test in GraphPad Prism software. A minimum of 100 cells were analyzed per batch for foci formation, followed by calculation of average foci in each group. **C.** Representative images depicting 53BP1 foci formation in HeLa cells upon treatment with SCR7-cyclized and SCR7-pyrazine (50 μ M and 100 μ M). 53BP1 is stained with FITC (green), whereas nucleus is counterstained using propidium iodide (red). The scale bar represents 0.2 μ m. **D.** Bar graph showing average 53BP1 foci in each group upon treatment with SCR7-cyclized and SCR7-pyrazine. **E.** Representative images showing direct double-strand break formation in Nalm6

cells as assessed using neutral comet assay (n=3). Cells were treated with SCR7-cyclized and SCR7-pyrazine (100 μ M and 250 μ M) for 24 h and processed for comet assay, followed by staining with propidium iodide. DMSO was used as a vehicle control. In case of each group, three independent images showing multiple cells have been presented. The scale bar represents 2 μ m. **F.** Scatter plot depicting tail moment of cells processed for neutral comet assay as analyzed using the CometScore software. A minimum of 50 cells were analyzed in each batch and the tail moment was plotted for control (grey), 100 μ M of SCR7-cyclized and SCR7-pyrazine (red), 250 μ M of SCR7-cyclized and SCR7-pyrazine (black), as a scatter plot showing mean \pm SEM (ns: not significant, *p < 0.05, **p < 0.005, ***p < 0.0001). In all cases, significance was calculated using the Student's t-test in GraphPad Prism software.

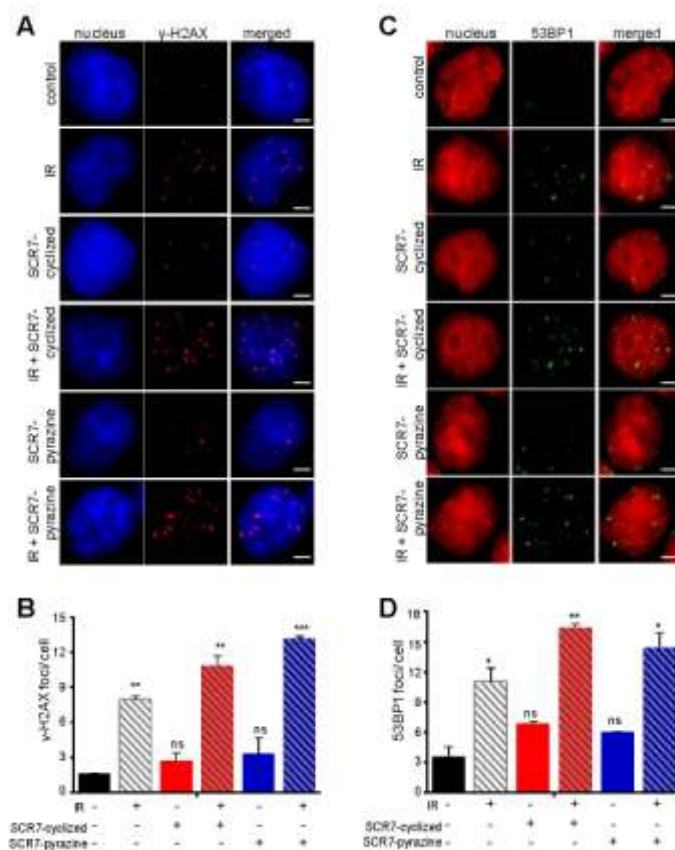


Figure 5

Figure 5. Accumulation of DNA breaks within the cells upon coadministration of IR and SCR7-cyclized or SCR7-pyrazine. **A.** Representative images of HeLa cells showing γ -H2AX foci upon treatment with IR (1 Gy) in conjunction with (or alone) SCR7-cyclized or SCR7-pyrazine (100 μ M) for 1 h. DMSO was used as vehicle control. γ -H2AX is detected using Alexa-fluor 568 (red), whereas nucleus is stained with DAPI (blue). In each case, merged image generated using ImageJ is presented. Each experiment was repeated (n=3). The scale bar represents 0.2 μ m. **B.** Bar graph showing average γ -H2AX foci in each group depicting mean \pm SEM (ns: not significant, *p < 0.05, **p < 0.005, ***p < 0.0001). In each case, a minimum of 100 cells were analyzed for foci formation and the cumulative data was presented as a bar graph. Significance was calculated using the Student's t-test in GraphPad Prism software. **C.** Representative images showing 53BP1 foci formation in HeLa cells upon irradiation (1 Gy) and SCR7-cyclized or SCR7-pyrazine treatment (100 μ M) for 1 h. 53BP1 foci are detected using FITC (green), nucleus is stained with propidium iodide (red). The scale bar represents 0.2 μ m. **D.** Bar graph depicting average number of 53BP1 foci in each cell. Each experiment was repeated (n=3), around 100 cells were analyzed per batch and the resulting cumulative data was plotted as a bar graph depicting mean \pm SEM (ns: not significant, *p < 0.05, **p < 0.005, ***p < 0.0001). In all cases, significance was calculated using the Student's t-test in GraphPad Prism software.

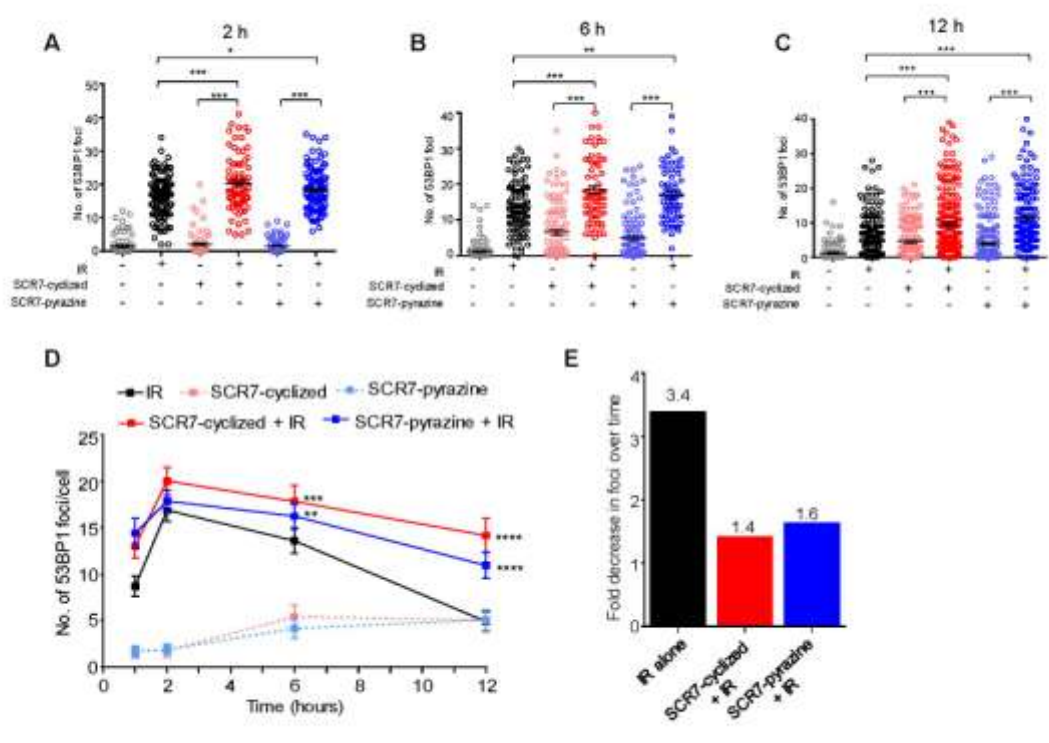


Figure 6

Figure 6. Assessment of DSB repair kinetics in cells following treatment with SCR7-cyclized or SCR7-pyrazine in combination with radiation. A-C. Scatter plots showing number of 53BP1 foci induced post treatment with radiation or inhibitors alone, and in combination, following a recovery period of 2 h (A), 6 h (B) and 12 h (C). ~100 cells were analysed in case of each sample (n=3) and plotted as scatter plot showing mean \pm SEM (ns: not significant, * $p < 0.05$, ** $p < 0.005$, *** $p < 0.0001$). In all cases, significance was calculated using the Student's t-test in GraphPad Prism software. **D.** Line graphs showing comparative analysis of 53BP1 foci plotted as a time-course post radiation in individual and combination treatments. Time points chosen for analysis were 1, 2, 6 and 12 h recovery post IR. Dotted lines represent SCR7-cyclized (red) and SCR7-pyrazine (blue) treatment, whereas solid lines depict IR alone (black), IR + SCR7-cyclized (red) and SCR7-pyrazine (blue). Statistical significance was calculated (Student's t-test) by comparing number of foci in IR alone, with that of IR and SCR7-cyclized or SCR7-pyrazine. **E.** Bar graph depicting fold change in number of 53BP1 foci over time (difference is compared between 2 h and 12 h). For each sample, fold decrease in the foci number was calculated at 2 and 12 h time points, and represented as individual bars for IR alone (black), IR + SCR7-cyclized (red) and IR + SCR7-pyrazine (blue).

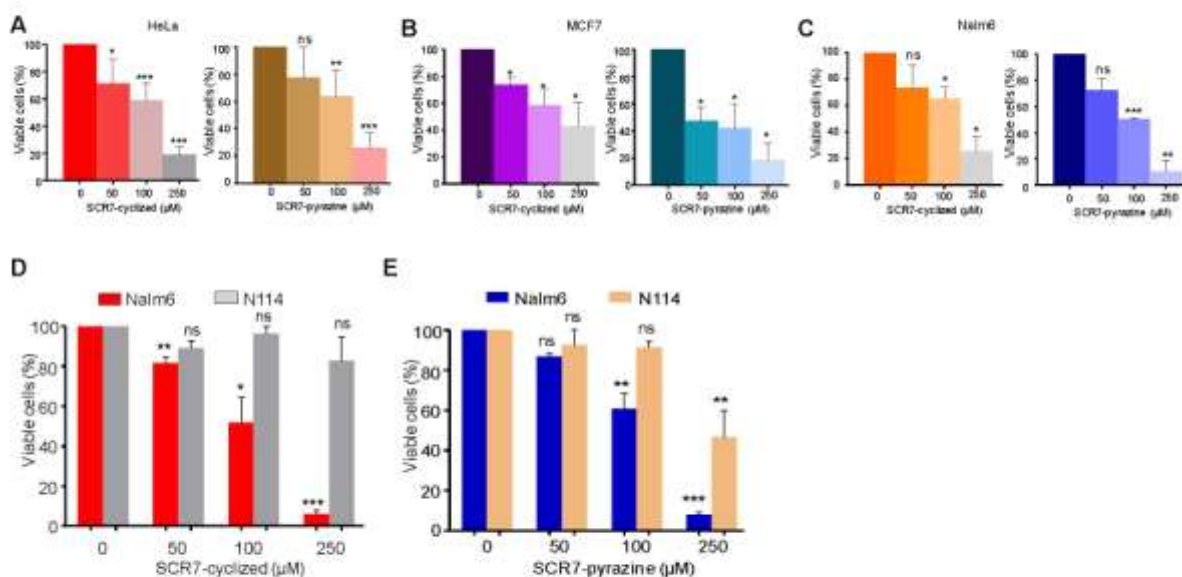


Figure 7

Figure 7. Effect of SCR7-cyclized and SCR7-pyrazine on cytotoxicity in cancer cell lines and in a Ligase IV knockout cell line. A-C. Bar graphs representing viable cells as assessed using trypan blue assay in HeLa (A), MCF7 (B) and Nalm6 (C) upon treatment with SCR7-cyclized and SCR7-pyrazine (50, 100 and 250 μM) for 48 h. Each experiment was repeated ($n=3$) and the percentage of viable cells was plotted as a bar graph showing mean \pm SEM. DMSO was used as a vehicle control. D,E. Bar graph showing comparative analyses of viable cells in case of Ligase IV knockout cell line, N114 and its wild type, Nalm6 cell line, following treatment with SCR7-cyclized (D) or SCR7-pyrazine (E) for 48 h. In each case, 50, 100 and 250 μM of inhibitor was used for treatment. DMSO was used as vehicle control. Each experiment was repeated ($n=4$) and the percentage viable cells plotted as a bar graph showing mean \pm SEM (ns: not significant, * $p < 0.05$, ** $p < 0.005$, *** $p < 0.0001$). In all cases, significance was calculated using the Student's t-test in GraphPad Prism software.

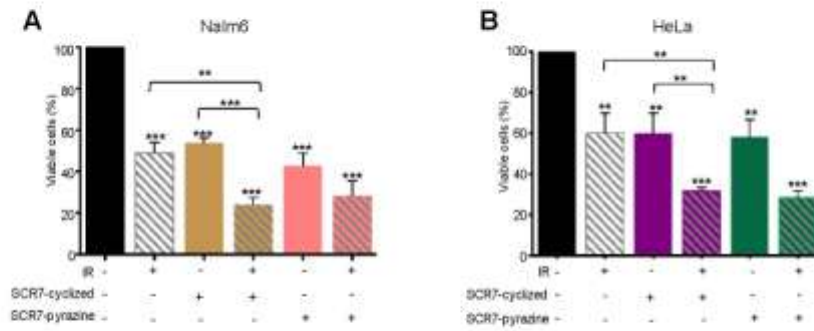


Figure 8

Figure 8. Evaluation of cytotoxicity upon coadministration of radiation and SCR7-cyclized or SCR7-pyrazine. A, B. Bar graph showing viable cells as assessed by trypan blue assay in Nalm6 (A) and HeLa cells (B) treated with radiation (1 Gy) in conjunction with SCR7-cyclized or SCR7-pyrazine (100 μ M) for 48 h. Each experiment was repeated (n=3) and the percentage of viable cells was plotted as a bar graph showing mean \pm SEM (ns: not significant, *p < 0.05, **p < 0.005, ***p < 0.0001). Significance was calculated using the Student's t-test in GraphPad Prism software.